Tension-Induced Straightening Transition of Self-Assembled Helical Ribbons

Brice Smith, Yevgeniya V. Zastavker, and George B. Benedek
Department of Physics, Center for Materials Science and Engineering and Materials Processing Center, Massachusetts Institute of Technology, Cambridge, Massachusetts 02139-4307
(Received 13 July 2001; published 10 December 2001)

Helical ribbons with pitch angles of either 11° or 54° self-assemble in a wide variety of quaternary surfactant-phospholipid/fatty acid-sterol-water systems. By elastically deforming these helices, we examined their response to uniaxial forces. Under sufficient tension, a low pitch helix reversibly separates into a straight domain with a pitch angle of 90° and a helical domain with a pitch angle of 16.5°. Using a newly developed continuum elastic free energy model, we have shown that this phenomenon can be understood as a first order mechanical phase transition.

DOI: 10.1103/PhysRevLett.87.278101 PACS numbers: 87.68.+z, 62.20.Dc

Self-assembled helical ribbons have been of increasing interest due to their potential use in applications ranging from drug delivery systems [1] to biological force probes. In addition, helical ribbons have been shown to be metastable intermediates in the process of cholesterol crystallization in the native gallbladder bile, the latter leading to the formation of gallstones [2,3]. In particular, Chung *et al.* found that in several model bile systems the helical ribbons formed had two distinctive pitch angles, 11.1° ± 0.5° and 53.7° ± 0.8° [4]. Zastavker *et al.* then showed that the formation of structures with these two distinct pitch angles was not unique to model biles, but was a general phenomenon of a variety of four-component systems composed of a bile salt or nonionic detergent, a phosphatidylcholine or fatty acids, a steroid analog of cholesterol, and water [5]. One of the new systems we choose to focus on is the chemically defined lipid concentrate (CDLC) from Gibco/BRL. In this commercially available system, the helical ribbons self-assemble with high yields and with high reproducibility.

The geometry of a helical ribbon is characterized by the ribbon width (w), thickness (t), contour length (s), helix radius (R), and pitch angle (ψ). We may also define the helix axial length as $\ell \equiv s\sin(\psi)$. We will define R_0, s_0, ℓ_0, and ψ_0 to be, respectively, the equilibrium radius, contour length, axial length, and pitch angle of a helix free from external stress. The low pitch helices in CDLC typically have an R_0 between 5 and 50 μm, an s_0 between 150 and 1500 μm, an ℓ_0 between 30 and 300 μm, and a w between 1 and 20 μm. In addition, we estimate the thickness to be 10–100 nm.

The helices are observed using an inverted microscope (Diaphot-TMD, Nikon) with phase contrast optics connected to a CCD camera (DXC-970MD, Sony). The images are recorded by a SVHS VCR (AG-1960, Panasonic) and then captured using the frame grabber on a Power Macintosh. The public domain NIH-Image software is then used to determine the helix geometric properties. We use Devcon 5-Minute Epoxy® to tether one end of a helix to a fixed rigid rod and the other to a movable cantilever or a rod attached to a piezoelectric micromanipulator (PCS-5000, Burleigh) which gives us precise control over the helix extension and compression.

In order to measure the force versus extension relationship, we use a nanofabricated silicon-nitride cantilever with an elastic constant of $(5.0 \pm 0.8) \times 10^{-5}$ N m^{-1} [6]. By simultaneously observing the cantilever deflection and the extension of the helix, we can determine the helix spring constant. Figure 1 shows a typical plot of the cantilever force versus helix extension. The spring constant of this particular helix ($R_0 = 19$ μm, $s_0 = 803$ μm, and $w = 12$ μm) is $(4.8 \pm 0.9) \times 10^{-6}$ N m^{-1}. For comparison, the spring constant of a lambda phage double-stranded DNA molecule is approximately 1 order of magnitude larger than this [7]. To within the uncertainty of the position measurements, our helix shows completely reversible and linear behavior.

As the external force is increased, the helix behaves like a conventional spring until the pitch angle reaches a value in the range of 16.5° to 25°. In this range a helix is mechanically metastable and, upon nucleation, the helix separates into two domains, one straight ($\psi_s = 90°$) and the other helical ($\psi_h = 16.5° \pm 1.3°$). These are connected by a crossover region whose length is typically on the order of R_0. The twist is relaxed through the condition

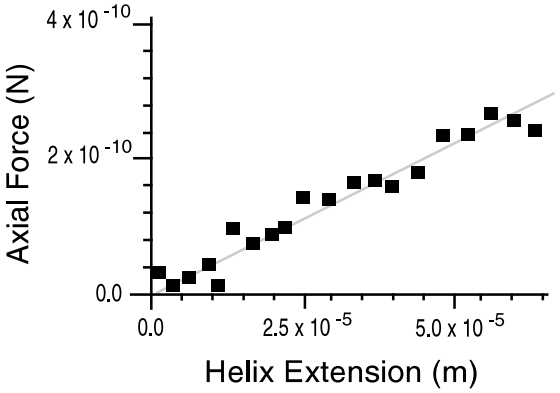

FIG. 1. Typical graph of cantilever force versus helix extension. The slope of the linear curve fit (4.8×10^{-6}) is the spring constant of this helix in N m^{-1}.

that our bond generates no torque on the system, allowing the helix to freely translate laterally along the epoxy's surface. Interestingly, like ψ_0, the pitch angle of the helical domain (ψ_h) is always the same regardless of the helix bulk geometry. A particular pulling sequence in one of the experiments is shown in Fig. 2.

The separation phenomenon, which occurs for all low pitch helices in CDLC, is perfectly reversible. Even if we increase the external force until a ribbon is torn apart while in a phase-separated state, both sections then relax to form helical segments of the same pitch angle and radius as the original complete helix. Together, all of these observations suggest that low pitch helices in CDLC undergo a first order phase transition where the pitch angle is the order parameter. This type of reversible tension-induced conformation change is analogous to the "stem-flower" transition observed in collapsed linear polymer systems [8], though the physical basis for the chain's transition is quite different from that of our system.

To formulate a description of this phase-separation phenomenon, we will consider the system to be entirely elastomechanical in nature. When free in solution, a ribbon is described by an internal elastic potential energy $F \equiv F(R, \ell, s)$. We will adopt the common nomenclature and henceforth refer to this as a free energy. To incorporate the effects of an externally applied uniaxial tension ($J_\parallel$), we may define the total energy of the system to be given by $W \equiv F - J_\parallel \ell$. (We have not included here the effects of an external torque in W because in our experiments no torque is applied.) Since the total contour length of the helix remains fixed, the equilibrium state of the system is found by minimizing W with respect to R and ℓ. This minimization results in the conditions that at equilibrium $(\partial F/\partial \ell)_{s,R} = J_\parallel$ and $(\partial F/\partial R)_{s,\ell} = 0$. The latter condition provides an expression for R in terms of ℓ and s, allowing R to be eliminated as an independent variable in our theory.

To describe the equilibrium of the phase-separated helix, we must consider the case when the total contour length is fixed but portions of it may be exchanged between regions of different pitch angles. The total W, given by $W_{\text{tot}} = W(s_s) + W(s_h)$ where $s_h = s_0 - s_s$, must be stable under a redistribution of the available contour length. Applying this stability constraint results in the equilibrium condition that $(\partial F/\partial s_s)_{\ell_s,R_s} = (\partial F/\partial s_h)_{\ell_h,R_h}$. This condition on mass exchange is equivalent to the condition of equal chemical potentials in the thermodynamic treatment of two-phase equilibrium. In light of this analogy, we will define $\tilde{\mu} \equiv (\partial F/\partial s)_{\ell,R}$ to be an effective contour length potential.

(a) (b) (c)

FIG. 2. (a) A low pitch helix free from external force attached to a glass rod at one end and surrounded by other free low pitch helices in solution, (b) the same helix attached at both ends and slightly extended, and (c) the helix extended beyond 16.5° and allowed to come to equilibrium with respect to the straightening transition (the helix ends are off screen).

Turning to a specific form for F, the free energy derived using an elastic continuum model is given by [9]

$$F(\psi, R, s) = sw\left(\frac{f(\psi)}{R^2} - \frac{K_s}{R}\right), \tag{1}$$

where $f(\psi) \equiv K_\alpha \cos^4(\psi) + 2K_\beta \cos^2(\psi)\sin^2(\psi) + K_\gamma \sin^4(\psi)$.

The $1/R^2$ term in Eq. (1) represents the elastic energy cost associated with deforming the ribbon away from a flat structure. The ribbon is modeled as a thin elastic material restricting us to consider only pure bends with zero Gaussian curvature. The local energy cost of such a deformation scales like the elastic modulus times the square of the deformation [10]. Since we will consider the ribbon to be anisotropic, there will in general be three phenomenologically determined elastic energy constants in our resulting free energy that will represent combinations of the components of the elastic modulus tensor. One coefficient (K_α) is associated with the bending of lines parallel to the contour length, another (K_γ) with bending of lines parallel to the width, and a third (K_β) with an additional energy cost due to coupling between the two primary deformations.

The $1/R$ term in Eq. (1) represents an intrinsic force within the ribbon that causes it to spontaneously bend. The choice of sign guarantees that the theory correctly predicts the experimental observation that only right-handed helices have been observed in CDLC. Using the equation for R derived from $(\partial F/\partial R)_{s,\ell} = 0$, it is possible to probe the form of this $1/R$ term by examining how the radius changes when a helix is deformed. Figure 3 shows our observation that there is a very weak dependence of R on ψ for small deformations. In fact, we find that R is independent of $\delta\psi \equiv \psi - \psi_0$ to first order. This observation requires the $1/R$ term to be independent of the pitch angle (i.e., the coefficient is simply a constant K_s). Our isotropic form for this term, analogous to a difference in surface tension between the ribbon's top and bottom, is in sharp contrast to previous theoretical models. Until now, models assuming that the chirality of the underlying molecules [11] or a spontaneous torsion of the edges [4] was responsible for this energy advantage have used a $1/R$ term proportional to $\sin(2\psi)$. Both of these models lead to a slope for the dashed line in Fig. 3 that is determined entirely by ψ_0, and is seen to be clearly inconsistent with our experimental findings.

Initially, the helices are free from external tension and torque which leads to the conditions $(\partial F/\partial \ell)_{s,R} = 0$ and

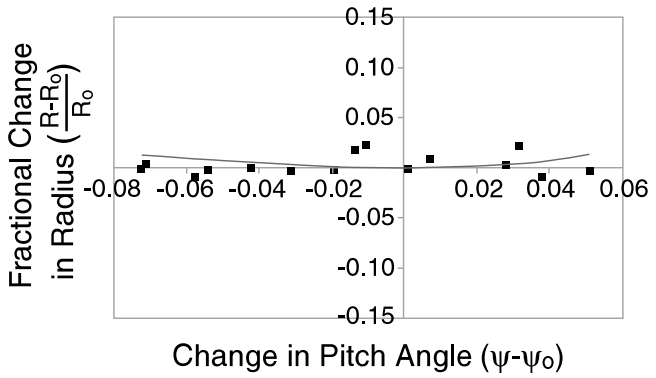

FIG. 3. Plot of typical experimental results for the fractional change in radius versus the change in pitch angle in radians (squares). Comparison with the theoretical results using an isotropic bending term (solid line) or using either a chiral or a spontaneous torsion model (dashed line).

$(\partial F/\partial R)_{s,\ell} = 0$. Applying these conditions to Eq. (1) allows ψ_0 and R_0 to be determined as follows:

$$\tan^2(\psi_0) = \frac{K_\alpha - K_\beta}{K_\gamma - K_\beta}, \tag{2}$$

$$R_0 = \frac{2}{K_s} f(\psi_0). \tag{3}$$

In the continuum elastic model, K_α, K_β, and K_γ in $f(\psi_0)$ are all expected to scale like the cube of the ribbon thickness [9,10]. Since K_s represents an isotropic surface force, it should not depend on the ribbon thickness. Thus, our theory suggests that the experimentally observed distribution in radii of helices with the same pitch angle is a reflection of a distribution in ribbon thickness.

For small deformations, the tension may be approximated by $J_\parallel(\ell, s_0) \approx K_{\text{spring}} \times (\ell - \ell_0)$, where $K_{\text{spring}} \equiv (\partial J_\parallel/\partial \ell)_s = (\partial^2 F/d\ell^2)_s$. Using this definition, the spring constant is found to be

$$K_{\text{spring}} = 8\,\frac{w}{R_0^2 s_0}\,(K_\alpha - K_\beta). \tag{4}$$

Examining Eq. (4), we note that, for the distribution of helix dimensions in CDLC, the spring constants can be expected to span more than 3 orders of magnitude. Using Eq. (4) and the data shown in Fig. 1, we obtain for this helix the value $K_\alpha - K_\beta = (1.5 \pm 0.6) \times 10^{-14}$ N m. It is important to reemphasize that this value depends on the thickness of the ribbon, but it provides a good indication of its order of magnitude in CDLC.

We can now return to the description of phase separation. Using $(\partial F/\partial R)_{s,\ell} = 0$ to eliminate R in favor of ψ in Eq. (1), a reduced free energy may be written as $\hat{F}(\nu) \equiv [F(\ell/s)/s]$, where $\nu \equiv \sin(\psi) = \ell/s$. Using this definition, the tension and effective contour length potential become $J_\parallel(\nu) = (d\hat{F}/d\nu)$ and $\tilde{\mu}(\nu) = \hat{F}(\nu) - \nu J_\parallel(\nu)$, respectively. The conditions $J_\parallel(\nu_h) = J_\parallel(\nu_s)$ and $\tilde{\mu}(\nu_h) = \tilde{\mu}(\nu_s)$ define the equilibrium values ν_h and ν_s. We may reexpress the condition for equilibrium with respect to material exchange as the following integral equation:

$$\int_{\nu_h}^{\nu_s} J_\parallel(\nu')\,d\nu' = J_\parallel(\nu_h) \times [\nu_s - \nu_h], \tag{5}$$

where the equality of the tensions is implicitly assumed. Figure 4 shows a plot of the theoretical tension versus ν curve and the resulting equilibrium construction which is equivalent to the equal area rule proposed by Maxwell for thermodynamic two-phase equilibrium [12].

We must, however, take care when applying these equilibrium conditions. At $\nu = 1$ the helix is straight and, therefore, no matter what additional force is applied, the pitch angle cannot increase. Thus the tension versus ν curve becomes vertical at $\nu = 1$ (see Fig. 4), automatically satisfying the condition of equal tensions between this point and ν_h. This fact provides the simple relation $\nu_s = 1$ which reduces Eq. (5) to a single equation for ν_h that depends only on the ratios (K_α/K_γ) and (K_β/K_γ). Therefore, our theory correctly predicts that the phase separation is entirely a property of the ribbon's underlying elastomechanical nature and thus completely independent of the helix bulk geometry.

Equations (2) and (5) provide two expressions for the two dimensionless ratios of elastic energy constants. In addition, Eq. (3) provides an expression for the third ratio of phenomenological coefficients in F. Using these equations, the values for the three ratios that do not depend on the ribbon thickness or on the helix radius or contour length are found to be

$$\begin{aligned}(K_\beta/K_\gamma) &= 0.000 \pm 0.015,\\ (K_\alpha/K_\gamma) &= 0.038 \pm 0.012,\\ (K_s R_0/K_\gamma) &= 0.073 \pm 0.022.\end{aligned} \tag{6}$$

These results have the following importance. First, the coupling between the two deformation modes (K_β) is

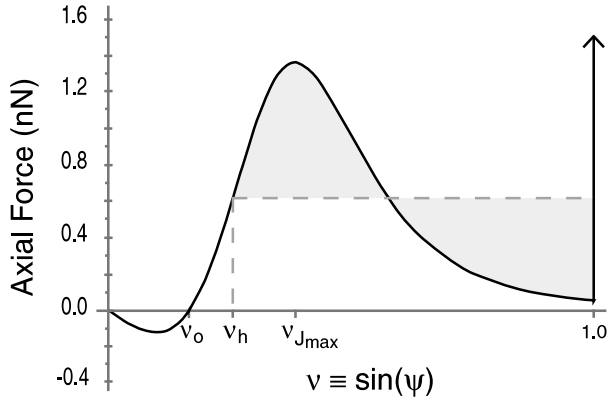

FIG. 4. Plot of a theoretical tension curve showing the equilibrium construction appropriate to our system. The figure also labels the free equilibrium value of ν [$\nu_0 = \sin(\psi_0) = 0.19$], the value of the order parameter in the helical phase ($\nu_h = 0.28$), and the limit of metastability with respect to the straightening transition ($\nu_{J_{\max}} = 0.42$).

equal to zero, restricting the symmetries that may exist in the ribbon microscopic structure. Second, our theory yields a value for the ribbon elastic anisotropy (K_α/K_γ) which is far more physically reasonable than that predicted by previous models [4,13]. This improvement stems from the fact that in our model the elastic anisotropy is given by $\tan^2(\psi_0)$, whereas in the previous models it scales as $\tan^4(\psi_0)$. Third, for the helix data shown in Fig. 1, the equilibrium value of the spontaneous bending energy per unit area (K_s/R_0) is found to be 8×10^{-5} N m^{-1}, roughly 100 times less than the surface tension of a fatty acid/water interface [14]. It is thus consistent to view this bending energy as arising from a difference in surface tension of the fatty acids which presumably coat the two sides of the ribbon [3,9].

As noted in the discussion following Eq. (4), K_{spring} provides a fourth equation for the coefficients, allowing absolute values to be determined for any helix. There is also a fifth relationship which allows for a check on the self-consistency of our results. This relationship gives the value of $\nu_{J_{\max}}$, the largest pitch angle which can be achieved before a helix becomes mechanically unstable (see Fig. 4). Using the values for the coefficient ratios in Eq. (6), the theoretical value of $\nu_{J_{\max}}$ is found to be 0.42 ± 0.06 corresponding to a pitch angle of 25°. Experimentally, we have measured $\nu_{J_{\max}}$ to be 0.41 ± 0.04, which is in excellent agreement with our model.

By elastically deforming self-assembled helices and measuring their response, we have obtained information on their elastic free energy. We have also discovered a novel tension-induced straightening transition for these structures. These experiments have led us to formulate a new model free energy using continuum elastic theory with an isotropic spontaneous bending term. With this model, we have been able to self-consistently explain all of the current experimental findings. By fitting measurements of ψ_0, R_0, and ψ_h to our theory, we have calculated the three geometry independent ratios of the coefficients in our model, and obtained their absolute values from the measurement shown in Fig. 1. In the future, repeating these experiments for helices formed in other systems will provide a powerful check of whether the universality of ψ_0 across a variety of chemical compositions is truly a reflection of a common microscopic structure. Finally, further characterization of the tethering process and of K_{spring} may open up the possibility of using these structures as self-assembled biological force probes.

We thank Professor G. Pollack of the University of Washington for donating the silicon-nitride cantilevers, Dr. A. Lomakin for his guidance in formulating the new continuum elastic model, and Dr. N. Asherie for his contributions to the understanding of the tension-induced phase transition. This work is supported by the Office of Naval Research under Grant No. N00014-95-1-0871.

[1] J. M. Schnur, Science **262**, 1669 (1993).
[2] J. M. Donovan and M. C. Carey, Gastroenterol. Clin. N. Am. **20**, 47 (1991).
[3] F. K. Konikoff, D. S. Chung, J. M. Donovan, D. M. Small, and M. C. Carey, J. Clin. Invest. **90**, 1155 (1992).
[4] D. S. Chung, G. B. Benedek, F. K. Konikoff, and J. M. Donovan, Proc. Natl. Acad. Sci. U.S.A. **90**, 11 341 (1993).
[5] Y. V. Zastavker, N. Asherie, A. Lomakin, J. Pande, J. M. Donovan, J. M. Schnur, and G. B. Benedek, Proc. Natl. Acad. Sci. U.S.A. **96**, 7883 (1999).
[6] M. E. Fauver, D. L. Dunaway, D. H. Lilienfeld, H. G. Craighead, and G. H. Pollack, IEEE Trans. Biomed. Eng. **45**, 891 (1998).
[7] S. B. Smith, Y. Cui, and C. Bustamante, Science **271**, 759 (1996).
[8] A. Halperin and E. B. Zhulina, Europhys. Lett. **15**, 417 (1991).
[9] Y. V. Zastavker, Ph.D. thesis, Massachusetts Institute of Technology, 2001.
[10] L. D. Landau and E. M. Lifshitz, *Theory of Elasticity* (Pergamon Press, Oxford, 1959).
[11] P. G. de Gennes, *The Physics of Liquid Crystals* (Oxford University Press, London, 1974).
[12] L. D. Landau and E. M. Lifshitz, *Statistical Physics* (Pergamon Press, Oxford, 1980).
[13] J. V. Selinger, F. C. MacKintosh, and J. M. Schnur, Phys. Rev. E **53**, 3804 (1995).
[14] S. E. Feller and R. W. Pastor, Biophys. J. **71**, 1350 (1996).